ADVANCED FUNCTIONAL MATERIALS

Supporting Information

for *Adv. Funct. Mater.,* DOI: 10.1002/adfm.202214945

All-Polymer Fiber Organic Electrochemical Transistor for Chronic Chemical Detection in the Brain

Jianyou Feng, Yuan Fang, Chuang Wang, Chuanrui Chen, Chengqiang Tang, Yue Guo, Liyuan Wang, Yiqing Yang, Kailin Zhang, Jiajia Wang, Jiawei Chen, Xuemei Sun, and Huisheng Peng**

Supporting Information

All-polymer fiber organic electrochemical transistor for chronic chemical detection in the brain

Jianyou Feng, Yuan Fang, Chuang Wang, Chuanrui Chen, Chengqiang Tang, Yue Guo, Liyuan Wang, Yiqing Yang, Kailin Zhang, Jiajia Wang, Jiawei Chen, Xuemei Sun, Huisheng Peng**

J. Feng, Y. Fang, C. Wang, C. Chen, C. Tang, Y. Guo, L. Wang, Y. Yang, K. Zhang, J. Wang, J. Chen, Prof. X. Sun, Prof. H. Peng
State Key Laboratory of Molecular Engineering of Polymers, Department of Macromolecular Science and Laboratory of Advanced Materials, Fudan University, Shanghai, 200438, China, E-mail: sunxm@fudan.edu.cn; penghs@fudan.edu.cn.

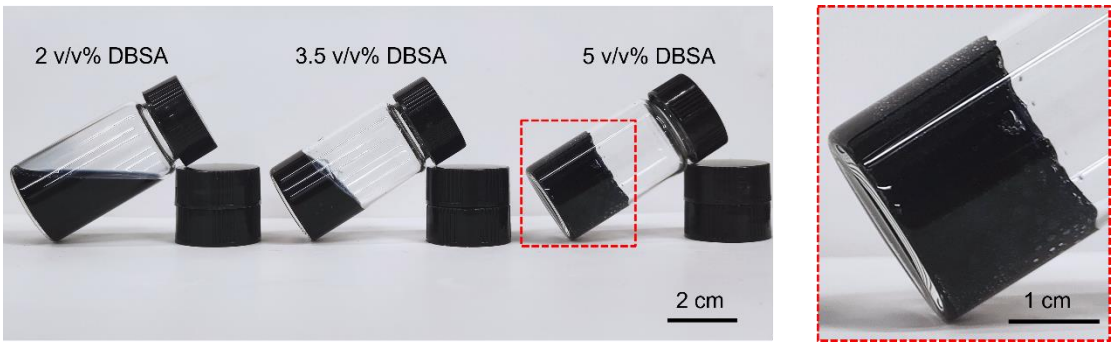

Figure S1. Photographs of the gelation of PEDOT:PSS containing 5 v/v% DMSO mixing with different volume ratio of DBSA. Right panel illustrates magnified view of red dotted box in left panel. The mixture solution containing 2 v/v% DBSA could not form gel. The mixture solution containing 3.5 v/v% DBSA formed gel after 30 minutes. The mixture solution containing 5 v/v% DBSA formed gel within 2 minutes, leading to gel containing a lot of bubbles which will hinder the solution extrusion process.

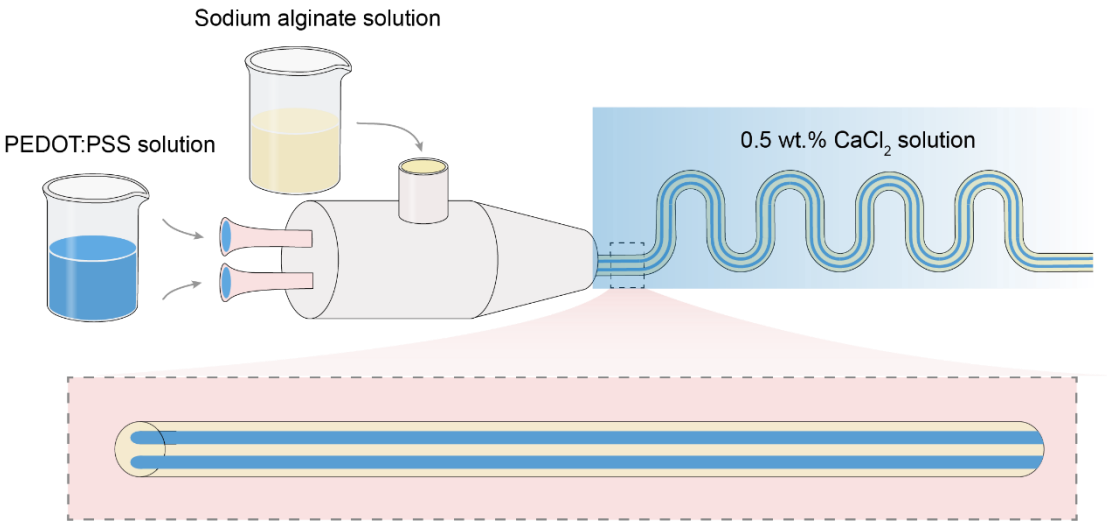

Figure S2. The schematic diagram for preparation of P-fibers. Sodium alginate and PEDOT:PSS solutions (mixture of pristine PEDOT:PSS, 5 v/v% DMSO and 3.5 v/v% DBSA) were simultaneously extruded from a three-channel spinneret into the 0.5 wt.% calcium chloride ($CaCl_2$) coagulation bath, and then coagulated.

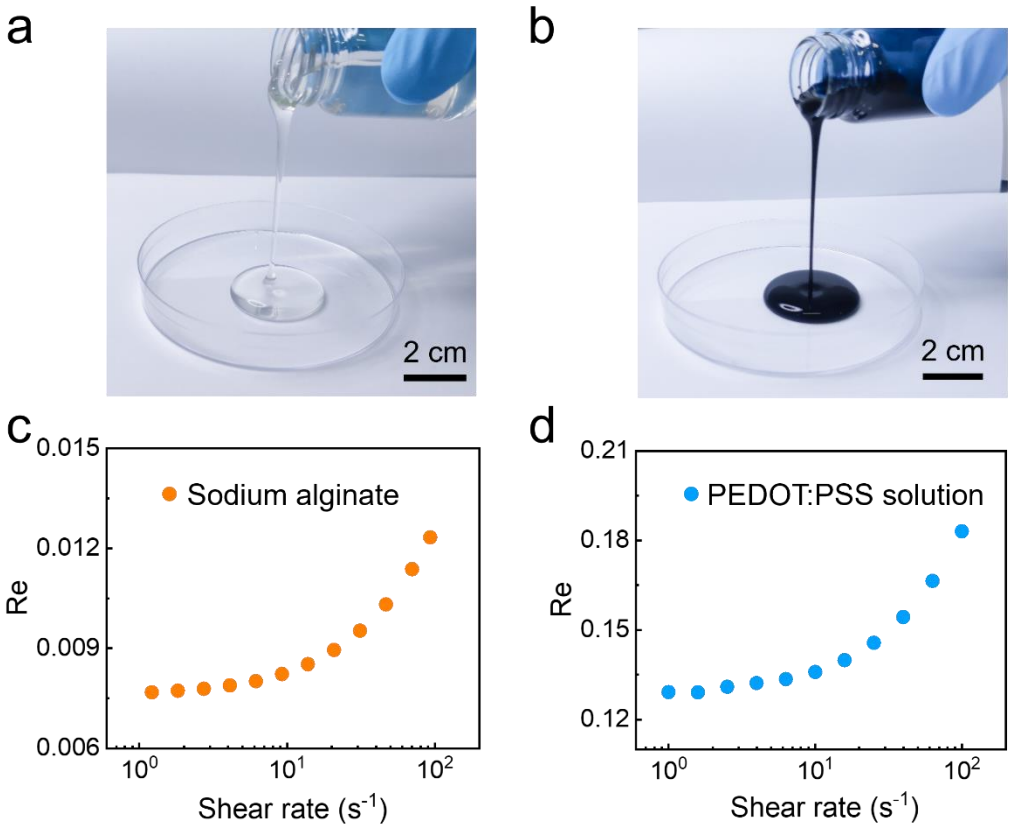

Figure S3. The rheological property of sodium alginate and PEDOT:PSS solution (mixture of pristine PEDOT:PSS, 5 v/v% DMSO and 3.5 v/v% DBSA). (a, b) Photographs of the sodium alginate and the PEDOT:PSS solution, respectively. (c, d) Reynolds number (Re) in relation to the shear rate for the sodium alginate and PEDOT:PSS solution, respectively.

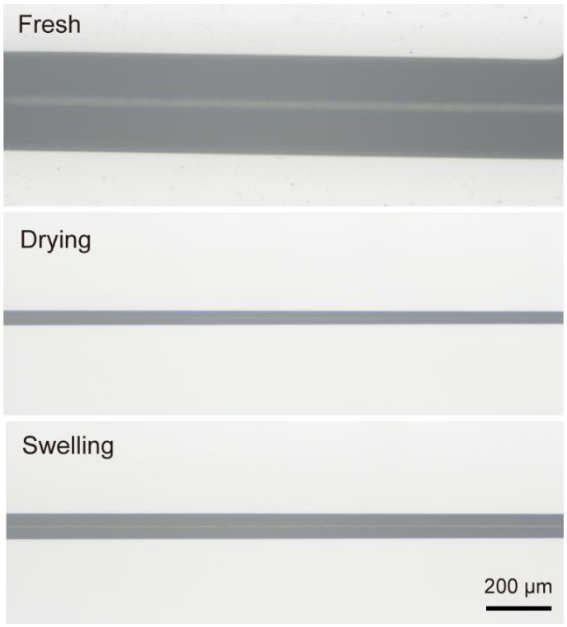

Figure S4. Photographs of P-fiber under different conditions.

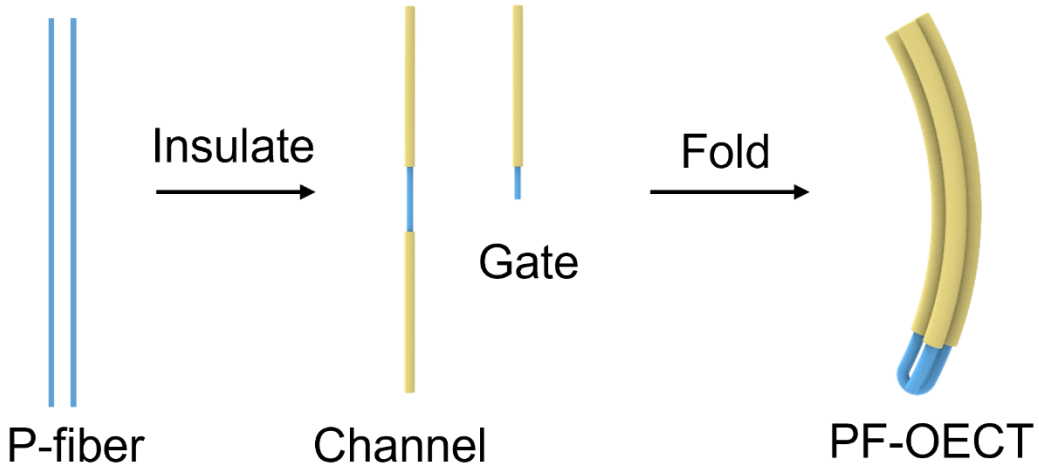

Figure S5. The preparation of PF-OECT. P-fibers were insulated with fluorine rubber and being folded to PF-OECT.

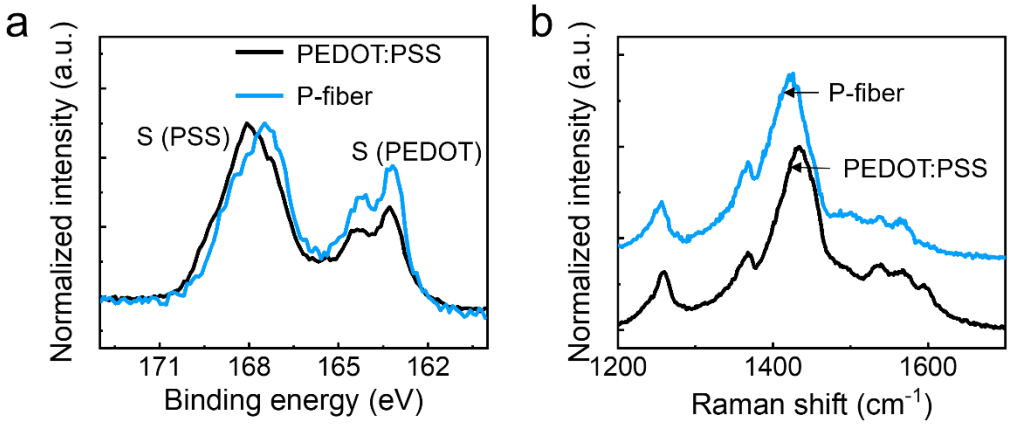

Figure S6. (a) S2p XPS spectra for PEDOT:PSS and P-fiber. (b) Raman spectra for PEDOT:PSS and P-fiber.

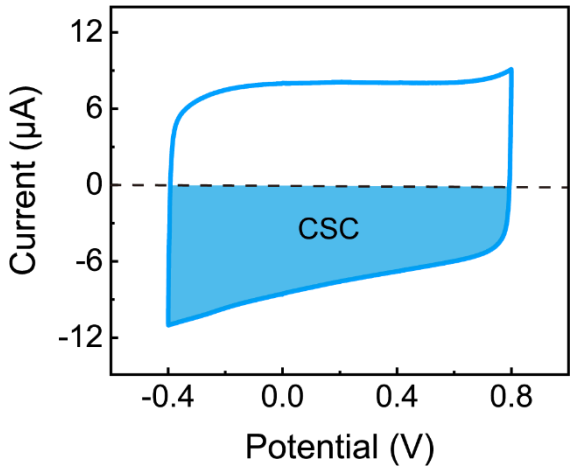

Figure S7. Representative cyclic voltammetry of the P-fiber in 1x PBS. Scan rate was 50 mV s^{-1}. CSC means charge storage capacity.

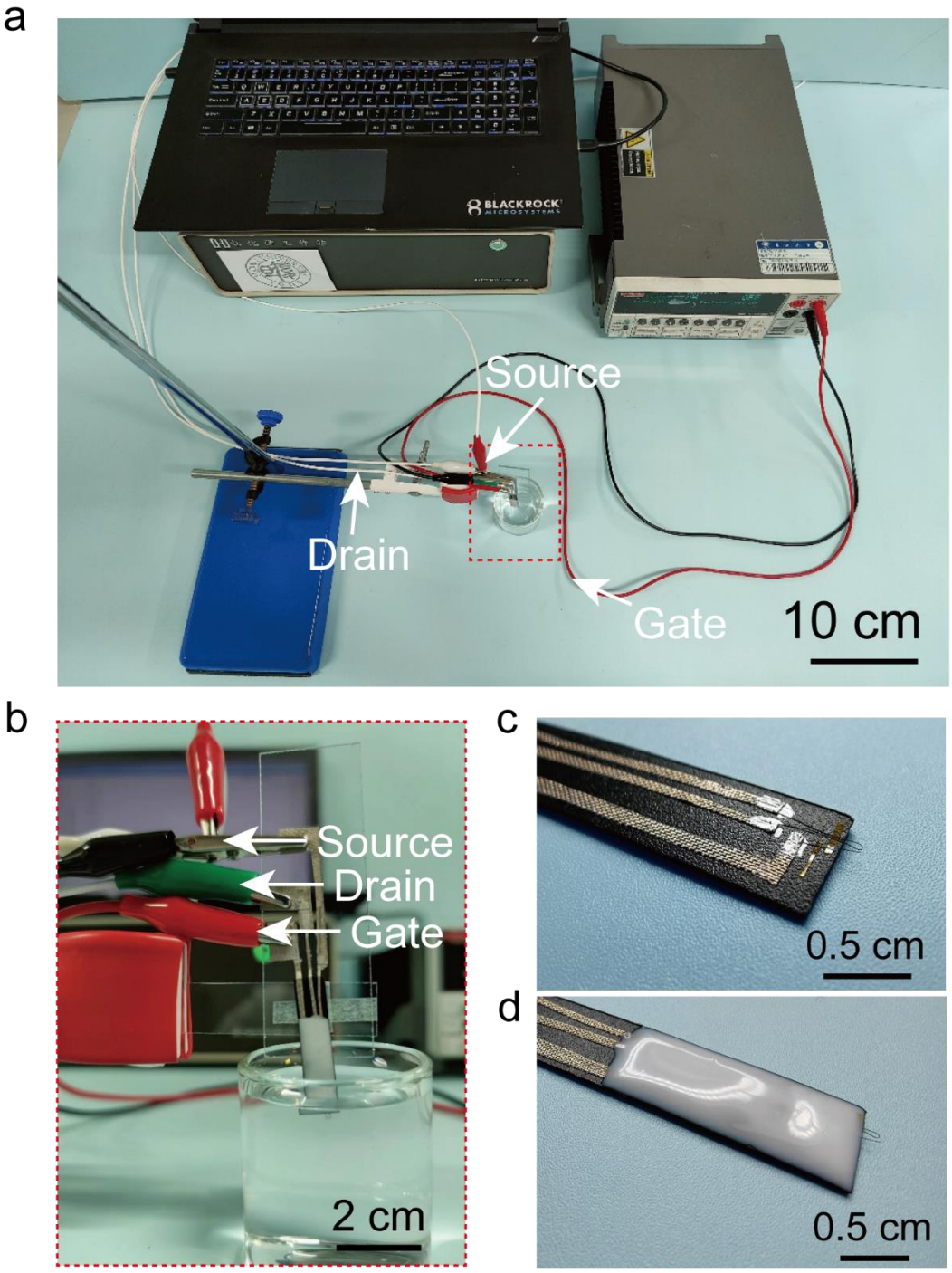

Figure S8. The PF-OECT connected to the acquisition system. (a) Photograph of PF-OECT connected to the acquisition system. (b) Photograph of PF-OECT immersing in an electrolyte. (c, d) The circuit connection of PF-OECT before and after insulation with silicone rubber.

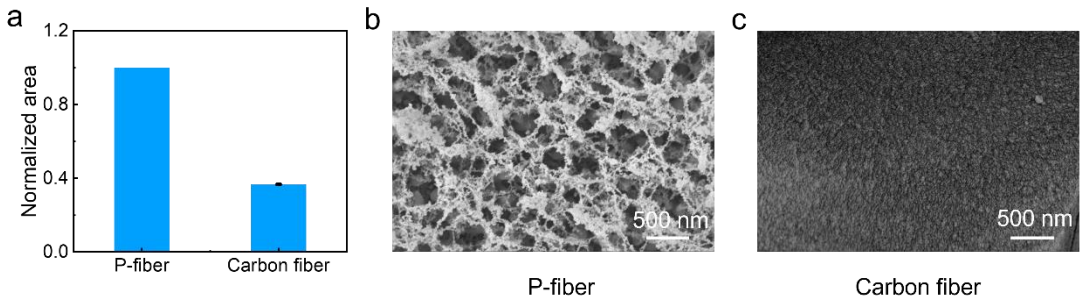

Figure S9. (a) Normalized electrochemical active areas of P-fibers and carbon fibers. (b) Scanning electron microscopy image of the cross section of P-fiber. (c) Scanning electron microscopy image of the cross section of carbon fiber.

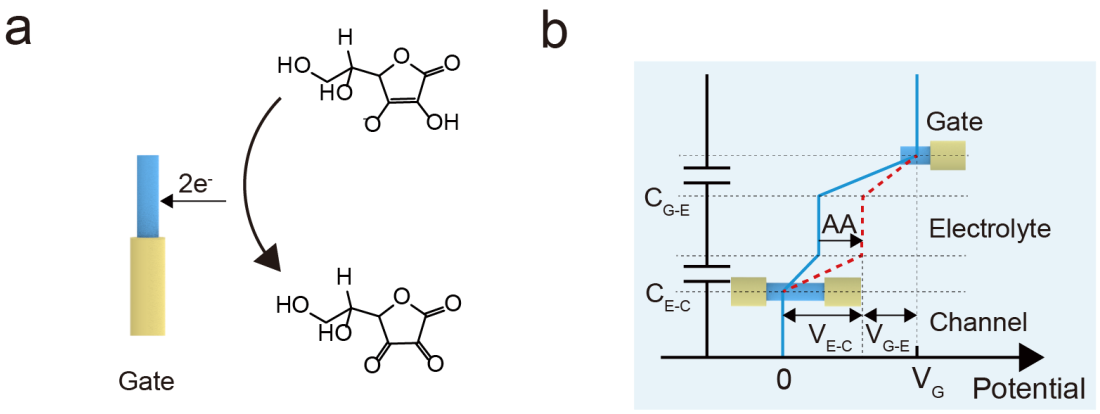

Figure S10. The working mechanism of PF-OECT in response to AA in an electrolyte. (a) Schematic of AA oxidation on the surface of the gate electrode. (b) Schematic of a PF-OECT working in the electrolyte along with potential drops before and after the addition of AA.

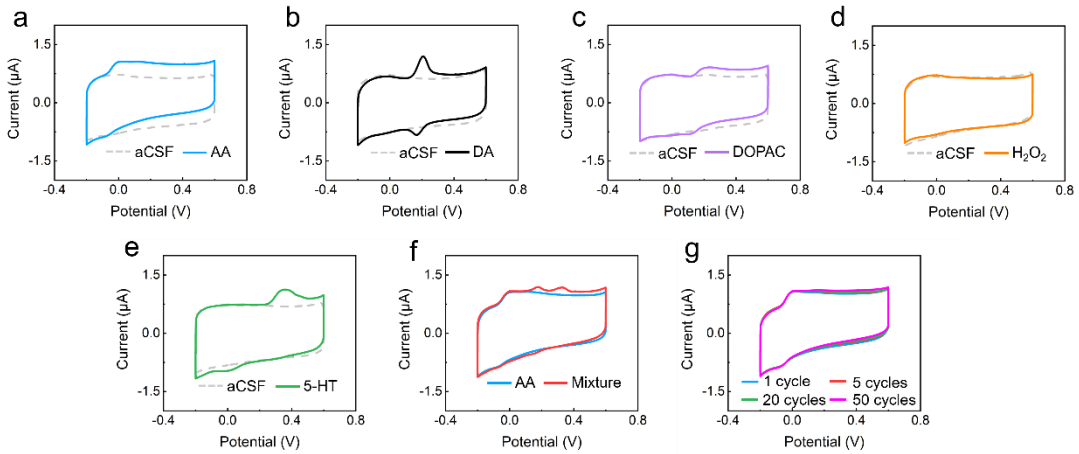

Figure S11. Cyclic voltammograms of the P-fiber in artificial cerebrospinal fluid (aCSF) containing different chemicals. (a) 0.2 mM ascorbic acid (AA). (b) 0.2 mM dopamine (DA). (c) 0.2 mM 3,4-dihydroxyphenylacetic acid (DOPAC). (d) 0.2 mM hydrogen peroxide (H_2O_2). (e) 0.2 mM serotonin (5-HT). (f) 0.2 mM AA and mixture solution of 0.2 mM AA, 20 μM DA, 20 μM DOPAC, 20 μM H_2O_2, 20 μM 5-HT. (g) 0.2 mM AA for different cycles. Scan rate was 5 mV s^{-1}.

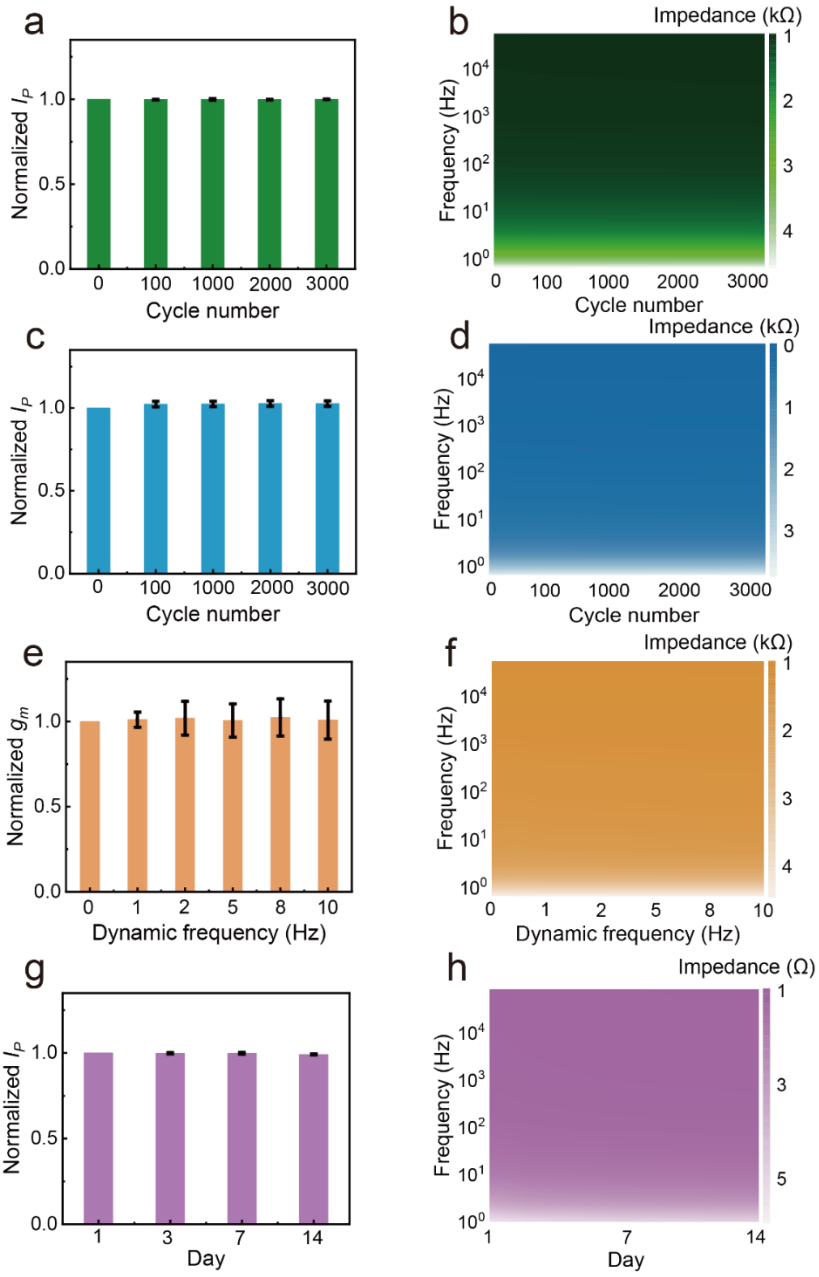

Figure S12. Stability of PF-OECT. (a, b) The normalized oxidation peak current and impedance of the gate electrode under bending for 3,000 cycles, respectively. (c, d) The normalized oxidation peak current and impedance of the gate electrode under twisting for 3,000 cycles, respectively. (e, f) The normalized transconductance of PF-OECT and impedance of the gate electrode at different dynamic frequencies under mechanical stirring to mimic the heartbeat and respiration, respectively. (g, h) The normalized oxidation peak current and impedance of the gate electrode soaking in artificial cerebrospinal fluid for 14 days, respectively.

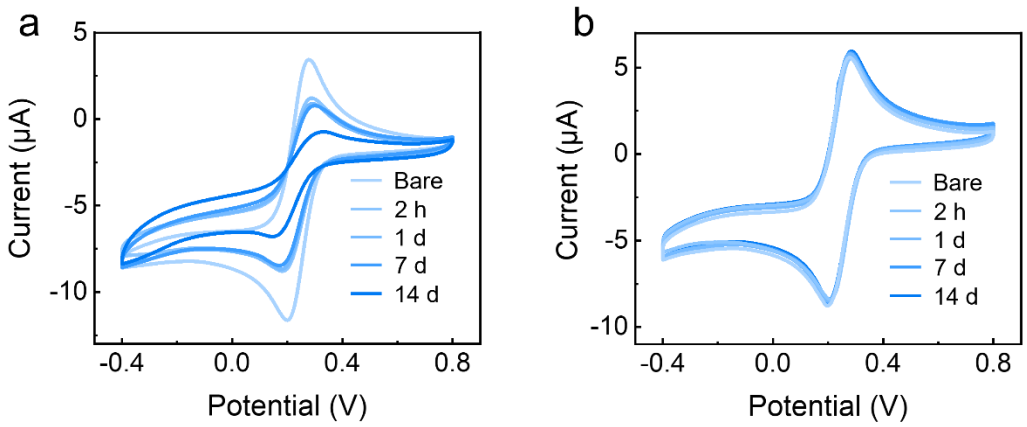

Figure S13. Biofouling of carbon fibers. (a) Cyclic voltammograms of carbon fiber in the potassium ferricyanide solution obtained before (bare) and after incubation in 10 mg mL^{-1} BSA solution for different periods. (b) Cyclic voltammograms of carbon fiber in the potassium ferricyanide solution obtained before (bare) and after incubation in artificial cerebrospinal fluid for different periods.

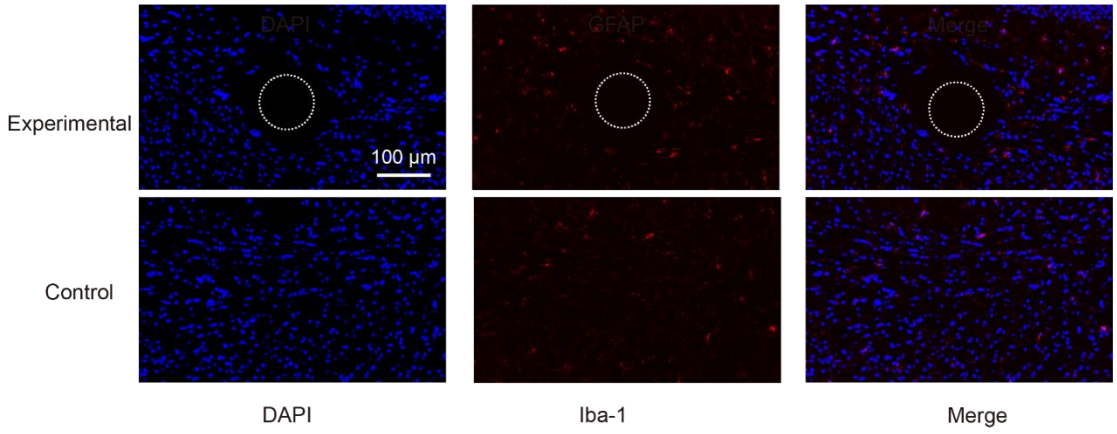

Figure S14. Biocompatibility of PF-OECT. Immunohistochemical staining images of brain slices at 14 days after implantation of PF-OECT and control group without implants. Blue and red correspond to 4′,6-diamidino-2-phenylindole (DAPI, label of cell nuclei) and ionized calcium-binding adapter molecule (Iba-1, label of microglia), respectively. The white dotted circle indicates the position of the PF-OECT.

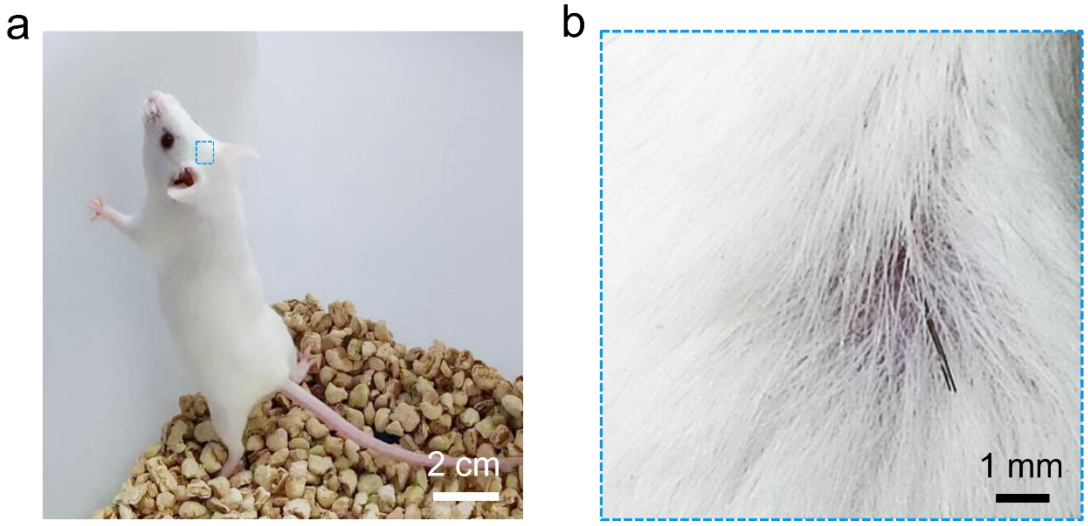

Figure S15. (a, b) Photographs of the mouse implanted with PF-OECTs at low and high magnifications, respectively.

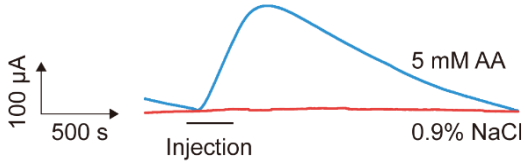

Figure S16. The detection ability of PF-OECT in the mouse brain. Real-time drain current of PF-OECT in mouse brain after intracerebral microperfusion of 2 μL 5 mM AA and 0.9 % NaCl solutions with a flow rate of 0.4 μL min^{-1}.

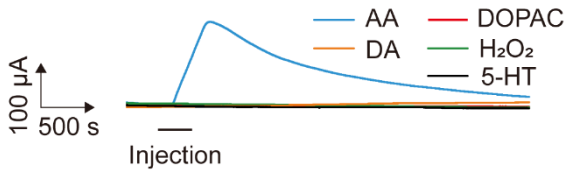

Figure S17. Selectivity of the PF-OECT measured *in vivo*. Real-time drain current of PF-OECT in mouse brain after intracerebral microperfusion of 2 µL 5 mM AA, 2 µL 100 µM DA, 2 µL 100 µM DOPAC, 2 µL 100 µM H_2O_2 and 2 µL 100 µM 5-HT solutions with a flow rate of 0.4 µL min^{-1}.

Table 1. Examples of recently reported implantable electrochemical sensors of AA.

Electrode materials	Electrochemical methods	Sensitivity	Implantation time	Ref
CF	CV	/	<1 d	[S1]
CF/MWNT	Amperometry	/	<1 d	[S2]
CF/MWNT	OCV	25 mV $(\lg([AA]\ M^{-1}))^{-1}$	<1 d	[S3]
CF/MWNT	DPV	0.48 μA mM^{-1}	<1 d	[S4]
CF/SWNT	Amperometry	/	<1 d	[S5]
CF/SWNT	Amperometry	/	<1 d	[S6]
CF/SWNT	GRP	26 mV $(\lg([AA]\ M^{-1}))^{-1}$	<1 d	[S7]
CF/SWNT	Amperometry, DPV	/	<1 d	[S8]
CF/VACNT	Amperometry, CV	/	<1 d	[S9]
CF/CNT/Nafion	Amperometry	42.6 pA μM^{-1}	<1 d	[S10]
CF/Nafion/CNT	Amperometry	/	<1 d	[S11]
CF/Co-TPFC/MWNT	Multi-potential step amperometry	/	<1 d	[S12]
CF/thionine/KB	CV	/	<1 d	[S13]
CF/PEGDGE/HRP/Nafion	CV	20 ± 8.6 pA μM^{-1}	<1 d	[S14]
CF/HA/CSs	Amperometry	/	<1 d	[S15]
LCPE	DPA	35 ± 7 nA mM^{-1}	<1 d	[S16]
Si/Ti/Au/SWNT	GRP	/	<1 d	[S17]
CNT fiber	DPV	0.85 mA mol^{-1} cm^{-2}	<1 d	[S18]
PEDOT:PSS	OECT	0.587±0.017 mA $(\lg([AA]\ M^{-1}))^{-1}$	14 d	This work

Abbreviation: CF: carbon fiber, MWNT: multi-walled carbon nanotube, SWNT: single-walled carbon nanotube, VACNT: vertically aligned carbon nanotube, CNT: carbon nanotube, Co-TPFC: cobalt corrole [Co(tpfc)(py)2] (tpfc=5,10,15-tris(penta-fluorophenyl) corrole, py = pyridine), KB: Ketjen black, PEGDGE: poly(ethylene glycol 400 diglycidyl ether), HRP: horseradish peroxidase type II, HA: heptylamine,

CSs: carbon nanospheres, LCPE: lipid treated carbon paste electrode, Si: silicon, Ti: titanium, Au: gold, CV: cyclic voltammetry, OCV: open-circuit voltage, DPV: differential pulse voltammetry, GRP: galvanic redox potentiometry, DPA: differential-pulse amperometry.

Reference

[S1] Y. Xue, W. Ji, Y. Jiang, P. Yu, L. Mao, *Angew. Chem. Int. Ed.* **2021**, 60, 23777.

[S2] J. Liu, P. Yu, Y. Lin, N. Zhou, T. Li, F. Ma, L. Mao, *Anal. Chem.* **2012**, 84, 5433.

[S3] P. Yu, H. Wei, P. Zhong, Y. Xue, F. Wu, Y. Liu, J. Fei, L. Mao, *Angew. Chem. Int. Ed.* **2020**, 59, 22652.

[S4] M. Zhang, K. Liu, L. Xiang, Y. Lin, L. Su, L. Mao, *Anal. Chem.* **2007**, 79, 6559.

[S5] T. Xiao, Y. Jiang, W. Ji, L. Mao, *Anal. Chem.* **2018**, 90, 4840.

[S6] T. Xiao, Y. Wang, H. Wei, P. Yu, Y. Jiang, L. Mao, *Angew. Chem. Int. Ed.* **2019**, 58, 6616.

[S7] F. Wu, H. Cheng, H. Wei, T. Xiong, P. Yu, L. Mao, *Anal. Chem.* **2018**, 90, 13021.

[S8] H. Cheng, T. Xiao, D. Wang, J. Hao, P. Yu, L. Mao, *J. Electroanal. Chem.* **2016**, 781, 90.

[S9] L. Xiang, P. Yu, J. Hao, M. Zhang, L. Zhu, L. Dai, L. Mao, *Anal. Chem.* **2014**, 86, 3909.

[S10] N. R. Ferreira, R. M. Santos, J. Laranjinha, R. M. Barbosa, *Electroanalysis* **2013**, 25, 1757.

[S11] N. R. Ferreira, A. Ledo, J. Laranjinha, G. A. Gerhardt, R. M. Barbosa, *Bioelectrochemistry* **2018**, 121, 142.

[S12] X. Liu, T. Feng, W. Ji, Z. Wang, M. Zhang, *Analyst* **2020**, 145, 70.

[S13] H. Cheng, X. Wang, H. Wei, *Anal. Chem.* **2015**, 87, 8889.

[S14] N. V. Kulagina, L. Shankar, A. C. Michael, *Anal. Chem.* **1999**, 71, 5093.

[S15] J. Jin, W. Ji, L. Li, G. Zhao, W. Wu, H. Wei, F. Ma, Y. Jiang, L. Mao, *J. Am. Chem. Soc.* **2020**, 142, 19012.

[S16] J. P. Lowry, M. G. Boutelle, R. D. O'Neill, M. Fillenz, *Analyst* **1996**, 121, 761.

[S17] H. Wei, L. Li, J. Jin, F. Wu, P. Yu, F. Ma, L. Mao, *Anal. Chem.* **2020**, 92, 10177.

[S18] L. Zhang, F. Liu, X. Sun, G.Wei, Y. Tian, Z. Liu, R. Huang, Y. Yu, H. Peng, *Anal. Chem.* **2017**, 89, 1831.